
# Experimental characterization of delamination in off-axis GFRP laminates during mode I loading

Lindgaard, Esben; Bak, Brian Lau Verndal

*Published in:*
Composite Structures

*DOI (link to publication from Publisher):*
10.1016/j.compstruct.2019.04.022

*Publication date:*
2019

*Document Version*
Early version, also known as pre-print

# Experimental Characterization of Delamination in Off-Axis GFRP Laminates during Mode I Loading

Esben Lindgaard*, Brian Lau Verndal Bak*

*Department of Materials and Production, Aalborg University, Fibigerstraede 16, DK-9220 Aalborg East, Denmark*

**Abstract**

This work experimentally investigates the influence of the off-axis angle between the lamina orientation and the crack growth direction in mode I delamination of GFRP laminates having R-curve behaviour due to large scale bridging. Initial and steady-state fracture toughness are characterized for different configurations of two laminate designs using moment loaded DCB specimens. In layup design 1, the layers adjacent to the initial delamination are parallel and the off-axis angle is varied. For layup design 2, only the off-axis angle of layers adjacent on one side of the initial delamination is varied. Microscopy, fractography, and comparisons of R-curves are used as tools to classify the cracking behaviour. All off-axis configurations tested experienced crack migration from the initial crack plane. In layup design 1, a significant difference in initial fracture toughness are found as opposed to layup design 2 in which an insignificant difference in initial fracture toughness and steady-state fracture toughness, respectively, are found. The off-axis configurations of layup design 2 are associated with crack migration and intraply crack propagation. The transition from interlaminar to intraply crack propagation correlates with the location of off-axis fibers not supported by the initial delamination indicating a free edge effect of the DCB specimen.

*Keywords:* Off-axis crack propagation, R-curve behaviour, Large scale bridging, Mode I delamination, Interlaminar fracture, Multidirectional laminated composite, Crack migration

## 1. Introduction

A common failure mode in laminated fibrous composite structures is damage of the interfaces between plies. This type of failure is called delamination and is one of the most dangerous and often seen damage modes in laminated composite structures [1]. Typically, interlaminar fracture toughness of laminated composites is characterized using simple unidirectional coupon specimens where the delamination is propagating along the fiber orientation [2]. However, in real structures delaminations cannot be guaranteed to propagate between and along unidirectional layers. In fact this special case is quite rare. This means that in order to perform delamination simulations of real structures using material properties obtained from these simple unidirectional coupon specimens alone, the assumption of isotropic fracture properties needs to be made.

Modelling and simulation of delaminations using the finite element method is available using e.g. interface elements and a cohesive model see [3–13]. Despite that cohesive models and finite elements have been enhanced greatly during the past decade they still rely on simplifications, which makes it questionable if they can be used for predicting delaminations in real 3D laminated composite structures [14]. The most important simplifications are 1) the delamination is predetermined to propagate at a given interface, 2) Mode II and Mode III crack loading is combined to a single shearing mode since current implementation cannot distinguish the two. 3) Isotropic fracture properties, which does not take the orientation of the adjacent layers into account. In order to formulate better and more realistic predictive tools it is vital to understand the delamination process of a broader spectrum of laminate configurations.

Previous studies of off-axis delamination, i.e. where crack growth direction is off-axis to surrounding lamina direction, and delamination of multidirectional laminates have primarily been focused on carbon fiber reinforced polymer (CFRP) laminates and initial fracture toughness at the onset of crack propagation, see the review by [15]. The influence of the off-axis angle in Mode I loading cases have been investigated by numerous researchers and the reported results show a significant variation of the influence of the off-axis angle. Examples of the largest relative differences between the initial fracture toughness for cracks propagating along the fiber orientation in relation to the fracture toughness obtained at off-axis angles up to 90° are: [16] 0%, [17] 47%, [18] 0%, [19] 100%, [20] 70%, [21] 64%, [22] -10%, [23] 40%, [24] -14%, [25] 0%. There has not been given much attention to the influence of the off-axis angle on the steady state fracture toughness for interfaces having a significant R-curve behavior. However, for glass fiber reinforced polymers (GFRP) the steady state fracture toughness has been reported to reach values more than four times larger the initial

☆Preprint version, final version available at https://doi.org/10.1016/j.compstruct.2019.04.022

*Corresponding author. Tel: +45 99407329; fax: +45 98151675

*Email addresses:* elo@mp.aau.dk (Esben Lindgaard), brianbak@mp.aau.dk (Brian Lau Verndal Bak)

fracture toughness at onset of crack propagation, see e.g. [26]. Thus, it is essential to characterize and include R-curve behavior when analysing or simulating crack propagation for GFRP laminates.

The objectives of the current study is to experimentally characterize delamination in off-axis GFRP laminates having large scale bridging, thus the whole R-curve is characterized in order to consider both the initial and the steady-state fracture toughness. The purpose of the study is to investigate the off-axis behavior of a specific glass-epoxy laminate to determine if it is feasible to apply state-of-the-art finite element simulation methods based on cohesive zone models with the limitations already mentioned. A number of different laminate configurations are examined in order to quantify the dependency of fracture properties with respect to interlaminar crack propagation direction as well as orientation of surrounding laminae. Double cantilever beam (DCB) specimens loaded by pure bending moments are used to experimentally characterize delaminations in two different overall laminate designs. In the layup of layup design 1 the layers adjacent to the delamination are parallel and the angle between the layers and the crack propagation direction is varied. For layup design 2 the angle between the layers adjacent to the delamination is varied. A newly developed test fixture [27] is applied in this work to produce pure bending moments to a DCB specimen by a wire and roller system. Fractography, i.e. examination of fracture surfaces, is applied as a tool to understand the cracking behaviour and the driving mechanisms during delamination.

The manuscript is organized in the following way. First the test setup, specimen design, and methods applied in the tests are described in Sec. 2. Then the results and discussion are presented for layup design 1 and layup design 2, respectively, in Sec. 3. Finally, conclusions are provided in Sec. 4.

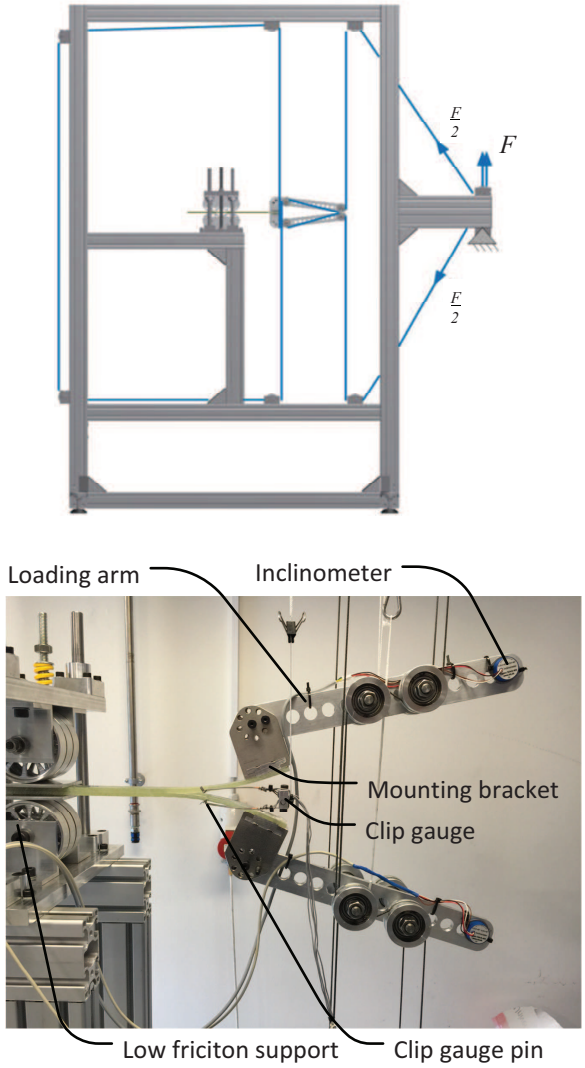


Figure 1: Overview of test fixture for mixed-mode bending test of DCB specimen with pure uneven bending moments.

## 2. Test setup and methods

### *2.1. DCB mixed-mode bending fixture*

For delamination testing of DCB specimens a newly developed special purpose test fixture introduced in [27] is applied. The test fixture, shown in Fig. 1, can produce pure even or uneven bending moments on DCB specimens based on a pure tensile loading input from a standard tensile testing machine. The concept of the test fixture is based on the principle from [28] where a string pulley system can introduce pure uneven bending moments on a double cantilever beam specimen. The developed test fixture is designed such that unwanted effects from large displacements and rotations are minimized which imply that the test fixture can be used to test more compliant and and thereby thinner DCB specimens. This is realized by redesigning the entire topology of the string pulley system, the roller support of the specimen, and also the orientation and attachment of the moment loading arms. It ensures that a pure moment can be introduced to the specimen even in conditions involving large displacements and rotations. Furthermore, the redesign of the string pulley system results in more compact test fixture than current available pure moment text fixtures. The test fixture is mounted in and actuated by standard tensile testing machines, thus using the actuation and high quality data acquisition system already available.

The basic outline of the fixture is as follows. The DCB specimen is mounted in a frictionless support achieved by lightweight rollers and ceramic bearings. In between the DCB specimen and roller support two aluminium plates are placed to ensure a smooth rolling surface, see Fig. 1. Two moment loading arms with rollers are attached to the specimen. The applied force couple to each of the moment loading arms is achieved by a wire and roller system using a single continuous wire, which ensures a constant wire force and thus identical force on each roller on the moment loading arm. The moment is a function of the magnitude of the force applied to the rollers and the horizontal distance between these. In order to calculate the horizontal distance between the rollers the angle of each loading arm are measured using inclinometers, cf. Fig. 1. A pretensioned braided Dyneema rope is used as wire due to its low weight, low friction, low bending stiffness, high tensile stiffness, and

high strength. A clip gauge is attached on pins mounted at the location of the initial crack tip of the DCB specimen and measures the crack end-opening displacement during fracture testing. For a detailed description and validation of the test fixture the reader is referred to [27].

### 2.2. Experimental data processing

The energy release rate for the moment loaded DCB specimen shown in Fig. 2 can be determined using solutions based on the J-integral approach [29], here assuming plane stress conditions, and which has been proven to also apply in large scale bridging cases [30],

$$G = J = \frac{21M_1^2 + 21M_2^2 - 6M_1M_2}{4EH^3W^2}, \quad \text{where} \qquad (1)$$

where $H$ is the height of each beam, $W$ is the width of the DCB specimen, $E$ is Young's modulus, and $M_1$ and $M_2$ are the applied moments on each arm of the DCB specimen, cf. Fig. 2. For all the tests reported here $M_1 = -M_2$ and $M_2 > 0$.

The fracture resistance curve also known as the R-curve for typical GFRP laminates starts with the initial fracture resistance associated with crack tip cracking and increases as the delamination crack grows due to fiber bridging effects appearing in the newly created crack surfaces, also known as the bridging zone. When the delamination crack has grown a certain amount the outermost bridging fibers in the wake of the delamination crack will fail and thus not transmit any forces. At this point the bridging zone has reached its maximum size and thus any further delamination crack propagation will be in a self-similar manner at a steady-state value for the fracture resistance, see Fig. 3.

The effects of delamination in off-axis GFRP laminates are here characterized by the initial fracture resistance $G_{c,o}$ which is defined here as the value of the J-integral at crack separation $\delta = 0.05$ mm and the maximum fracture resistance $G_{c,max}$, see Fig. 3. The crack separation for defining the initial fracture resistance has been found to correspond well with visual inspection during testing and the nonlinearity in the moment clip gauge relationship. The reason that the steady state fracture resistance $G_{c,ss}$ is not applied is that it is difficult to quantify due to the non-smooth shape of the resistance curves obtained in the tests.

### 2.3. Material and specimen configurations

Two GFRP laminate designs have been considered in this study, see Fig. 4. Layup design 1 is for testing the influence of the relative orientation of the adjacent layers to the initial

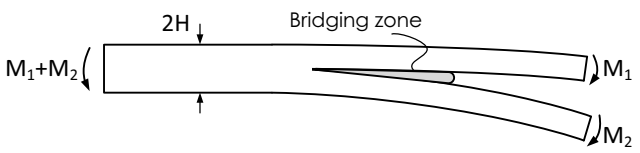


Figure 2: Definition of DCB specimen loaded with uneven pure bending moments.

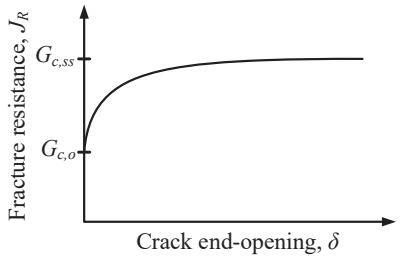


Figure 3: Fracture resistance, $J_R$, as function of crack end-opening, $\delta$, typically observed in delamination of GFRP laminates.

delamination on the R-curve at two different specimen widths. Layup design 2 is for testing the influence on the R-curve of the relative orientation of adjacent layers on only one side of the initial delamination crack and having crack propagation limited to those layers.

Both laminate designs consist of two outer sublaminates made from biaxial 50/50, 0°/90° noncrimp fabric mats with a weight of 800 g/m$^2$ (BIAX layers), a center sublaminate of unidirectional mats with a weight of $200 g/m^2$ (UD layers), and a $0.13\mu m$ thick PTFE film, which is used to produce an initial sharp crack. The nominal dimensions and layup of each specimen are given in Tab. 1.

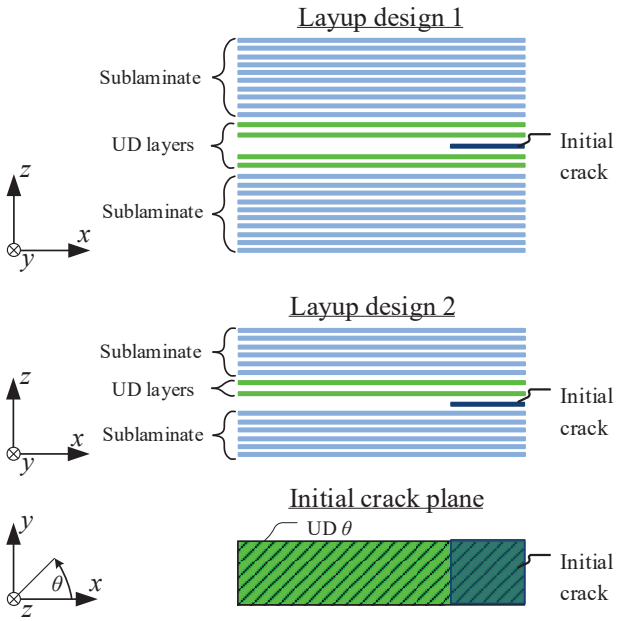


Figure 4: Layup definition of the two considered GFRP laminate designs. Definition of the off-axis angle $\theta$ is given as the orientation of the unidirectional plies surrounding the initial crack.

In layup design 1 the initial crack is surrounded by the UD plies which are considered at two configurations, i.e. $\theta = 0°$ and $\theta = 90°$. Furthermore, DCB specimens are cut at two widths in order to investigate any width dependency concerning delamination. In layup design 2 the initial crack is positioned between the UD plies and the BIAX mat. Here four different configurations are considered for off-axis delamination having the UD

| Layup design | Specimen type | Number of specimens | Layup | Width, $W$ [mm] | Height, $H$ [mm] |
|---|---|---|---|---|---|
| 1 | 1 | 2 | [$BIAX_{10}$@(0°,90°) / $UD_2$@0° / PTFE / $UD_2$@0° /$BIAX_{10}$@(90°,0°)] | 30 | 14.1 |
| 1 | 2 | 3 | [$BIAX_{10}$@(0°,90°) / $UD_2$@90° / PTFE / $UD_2$@90° /$BIAX_{10}$@(90°,0°)] | 30 | 14.1 |
| 1 | 3 | 2 | [$BIAX_{10}$@(0°,90°) / $UD_2$@0° / PTFE / $UD_2$@0° /$BIAX_{10}$@(90°,0°)] | 60 | 14.1 |
| 1 | 4 | 2 | [$BIAX_{10}$@(0°,90°) / $UD_2$@90° / PTFE / $UD_2$@90° /$BIAX_{10}$@(90°,0°)] | 60 | 14.1 |
| 2 | 5 | 4 | [$BIAX_6$@(90°,0°) / PTFE / $UD_2$@0° /$BIAX_6$@(0°,90°)] | 25 | 9 |
| 2 | 6 | 5 | [$BIAX_6$@(90°,0°) / PTFE / $UD_2$@30° /$BIAX_6$@(0°,90°)] | 25 | 9 |
| 2 | 7 | 5 | [$BIAX_6$@(90°,0°) / PTFE / $UD_2$@60° /$BIAX_6$@(0°,90°)] | 25 | 9 |
| 2 | 8 | 5 | [$BIAX_6$@(90°,0°) / PTFE / $UD_2$@90° /$BIAX_6$@(0°,90°)] | 25 | 9 |

Table 1: Layup and nominal dimensions of the test specimens. The actual measured dimensions have been used in the data processing of the results presented through out the paper.

plies oriented at $\theta = \{0°, 30°, 60°, 90°\}$. Please note that in layup design 2, as opposed to layup design 1, that the BIAX layers are flipped such that the initial crack is placed between differently oriented UD plies and the 0° ply in the BIAX mat.

In all configurations a relatively thick sublaminate consisting of BIAX mats has been applied in order to minimize the bend-twist coupling effects in the laminate while maintaining a simple and comparable layup for all the specimens tested. Coupling effects have been considered by studying the laminate ABD-matrices and 3D finite element static stress analyses using quadratic solid elements of the DCB specimens to ensure validity of the plane conditions in using Eq. (1).

Each DCB specimen is fitted with a pair of brackets for mounting the loading arms of the text fixture, see Fig. 1. These brackets are mounted by four M4 bolts in threaded holes on each of the DCB arms. Additionally, two pins are attached on the side of each DCB specimen at the location of the initial crack tip for the attachment of the clip gauge during testing, see Fig. 1 and Fig. 9.

The laminates have been manufacturing by the vacuum assisted resin transfer molding process using a PRO-SET INF114-INF213 [31] standard infusion epoxy and post-cured according to resin manufacturer specifications. The DCB specimens have been cut to dimensions using a diamond circular saw. The dimensions of each specimen have been measured using a caliber and the bending stiffness have been determined using a three point bending test on the actual specimens prior to fracture testing. These dimensions and the bending stiffness have been used to determine the R-curves presented in Sec. 3.

## 3. Results and discussion

### 3.1. Layup design 1

The fracture resistance curves for layup design 1 specimens are shown in Fig. 5 for nominal width $W = 30$ mm and in Fig. 6 for nominal width $W = 60$ mm.

Considering the overall trend of the fracture resistance curves for both widths it is apparent that the off-axis angle $\theta = 0°$ of the UD plies surrounding the initial crack produce quite smooth fracture resistance curves with considerable R-curve behaviour due to fiber bridging effects. The fracture resistance curves for the off-axis angle $\theta = 90°$ on the other hand are associated with

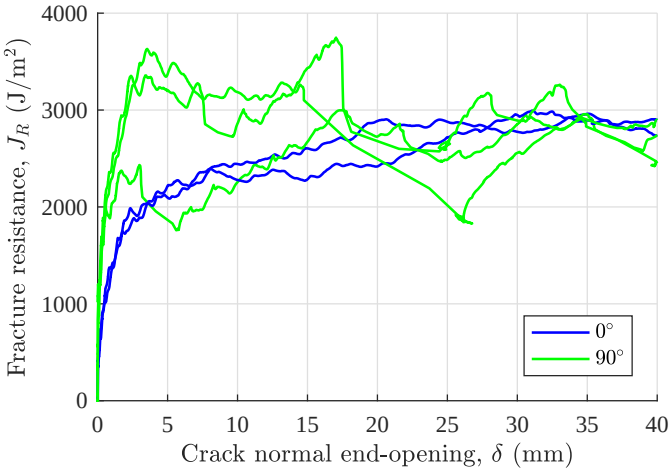


Figure 5: Fracture resistance curves for layup design 1, with nominal width $W = 30$ mm, off-axis angles $\theta = \{0°, 90°\}$.

large fluctuations and unstable crack growth. By fractography and inspection of the produced delamination crack in the DCB specimens having an off-angle of $\theta = 90°$, the fluctuations in fracture resistance is found to be caused by crack migration between the different interfaces during delamination testing, see Fig. 7. It was observed that the delamination crack migrates from the initial UD/UD interface towards an interface within the first BIAX mat by which the 0° ply in that BIAX mat restricts it from migrating further into the sublaminate. The process of crack migration of the 90° off-angle specimens are schematically illustrated in Fig. 8.

The initial fracture toughness $G_{Ic,o}$ and maximum fracture toughness $G_{Ic,max}$ are presented in Tab. 2. Here the first number represents the specimen type, cf. Tab. 1, and the last number is the specimen number. The initial fracture toughness $G_{Ic,o}$ is about twice as high for the specimens having an off-axis angle of $\theta = 90°$ compared to the $\theta = 0°$ specimens. This is probably caused by the complicated fracture process of the off-angled specimens where the delamination crack has to propagate through interlocked transversely oriented fibers having a propagation path not directly dictated by clear boundaries as is the case when the propagation plane and growth direction is bounded by surrounding 0° fibers.

For two out of the three 90° off-angled specimens shown

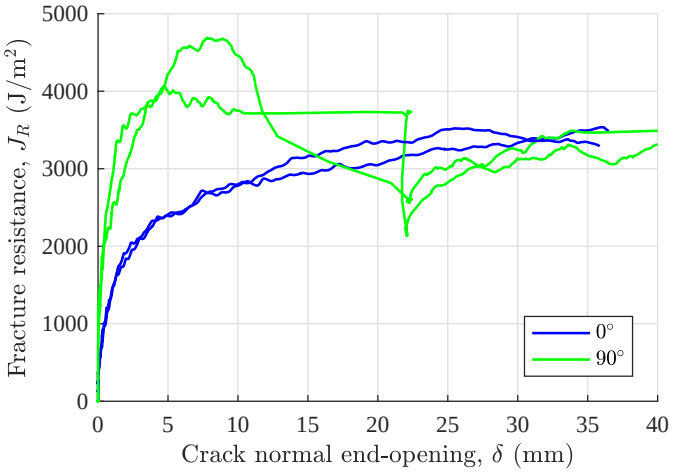


Figure 6: Fracture resistance curves for layup design 1, with nominal width $W = 60mm$, off-axis angles $\theta = \{0°, 90°\}$.

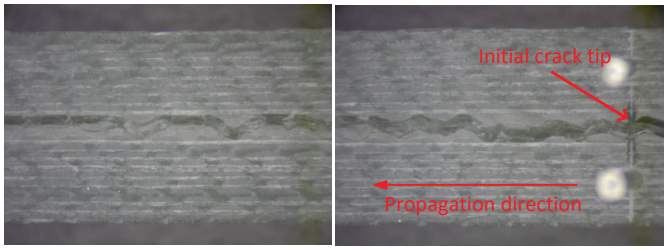


Figure 7: Fractographic inspection of delamination crack in layup design 1, with width of $W = 30mm$, off-angle $\theta = 90°$, and mode I loading. Initial crack tip and crack growth direction are marked on the specimen.

in Fig. 5, some steady-state crack propagation (for crack normal end-openings of $\delta = [3, 17]$ mm) in the UD/UD interface appeared before the delamination crack migrated to the interface within the first BIAX mat. The fracture toughness measured in this first region is higher than the steady-state fracture toughness $G_{Ic,ss}$ of the non off-angled specimens. The same observations were done for the 60mm wide specimens shown in Fig. 6. When considering the maximum fracture resistance of the 90° off-angle specimens in Fig. 6 with the ones in Fig. 5 there is more than 20% difference. The only difference between the specimens is the nominal width and indicates that the fracture process is dependent on the width of the specimens. The fiber bridging effects and microscopic imaging of the produced delamination crack during testing reveal a complicated fracture process, see Fig. 9. Here two distinct and separated zones of fiber bridging is identified, i.e. fiber bridging in a zone adjacent to the initial precrack, followed by a zone without any fiber bridging, and then a fiber bridging zone adjacent to the current crack tip. For the $\theta = 90°$ off-axis angled specimens the initial fiber bridging in the UD/UD interface is in the transverse direction to the crack growth direction(width direction of the DCB specimen). At some point the crack migrates outside the UD plies and continues at a specific interface in a BIAX mat where there is less fiber bridging. Since the initial fiber bridging in the UD/UD interface is associated with fibers bridging the fracture surface in the width direction this may explain the observed width dependency of the measured fracture resistance.

| Specimen | Off-axis angle | $G_{Ic,o}$ [J/m$^2$] | $G_{Ic,max}$ [J/m$^2$] |
|---|---|---|---|
| 1.1 | 0° | 449 | 2962 |
| 1.2 | 0° | 350 | 2993 |
| 2.1 | 90° | 1173 | 2998 |
| 2.2 | 90° | 799 | 3748 |
| 2.3 | 90° | 1036 | 3631 |
| 3.1 | 0° | 397 | 3536 |
| 3.2 | 0° | 413 | 3521 |
| 4.1 | 90° | 1307 | 4064 |
| 4.2 | 90° | 1013 | 4688 |

Table 2: Calculated initial fracture toughness $G_{Ic,o}$ and maximum fracture toughness $G_{Ic,max}$ for all layup design 1 specimens.

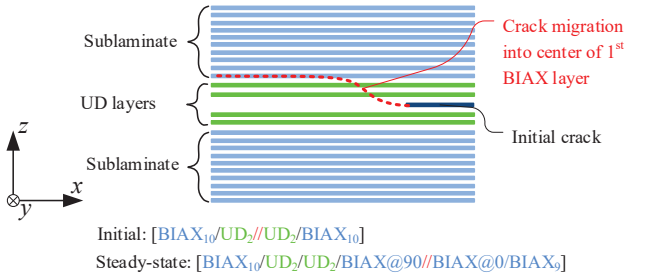


Figure 8: Illustration of the crack migration during crack propagation of the 90° off-axis angle layup design 1 DCB specimens. The symbol // is used to indicate the interface location of the crack within the stacking sequence for the initial and steady-state process of crack propagation.

### 3.2. Layup design 2

The fracture resistance curves for the layup design 2 specimens are shown in Fig. 10. The initial fracture toughness $G_{Ic,o}$ and the maximum fracture toughness $G_{Ic,max}$ for the layup design 2 specimens are given in Tab. 3. All specimens have a significant R-curve behaviour due to extensive fiber bridging in all DCB specimen configurations. From Fig. 10 the initial fracture toughness $G_{Ic,o}$ and steady-state fracture toughness $G_{Ic,ss}$, respectively, are similar across the different off-axis configurations. However, the characteristics of the fracture resistance curves across off-axis configurations are very different, i.e. the non off-axis configuration display smooth fracture resistance curves and a stable steady-state behaviour when the bridging zone is fully developed. The fracture resistance curves of all off-axis configurations display more fluctuations.

Fractography of the different off-axis configurations of layup design 2 reveal very different fracture morphology and fiber bridging effects, see Fig. 11. The non off-axis configuration with $\theta = 0°$ shows that delamination is *interlaminar* at the initial UD@0°//BIAX@0° interface, i.e. the delamination crack is restricted to propagate between the 0° plies. This process of delamination is illustratively shown on the top sketch in Fig. 12. Inspection of the fracture surfaces of the off-axis configurations with $\theta = \{30°, 60°, 90°\}$ shows *intraply* delamination with oscillating crack propagation in off-axis UD plies bounded by the

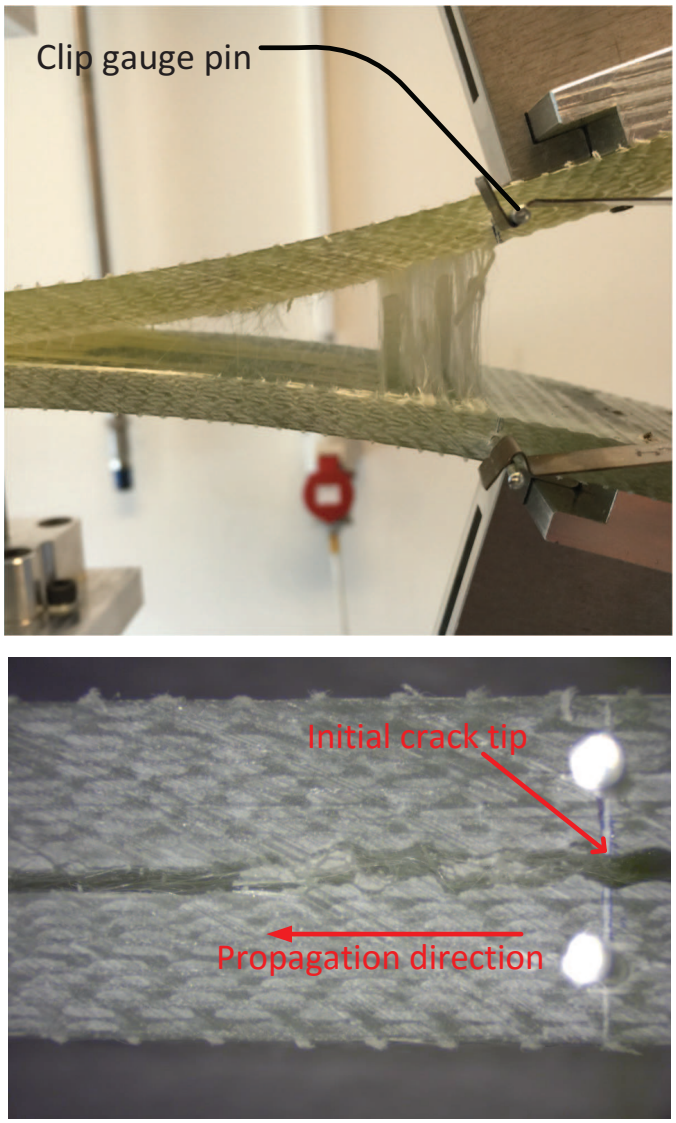


Figure 9: Layup design 1 with nominal width $W = 60mm$, $\theta = 90°$, and mode I loading. Top: Fiber bridging effects during testing. Bottom: Fractographic inspection of delamination crack. Initial crack and crack growth direction of the specimen is marked.

neighboring 0° ply of the BIAX mats. This observed delamination process is shown on the bottom sketch of Fig. 12.

By microscopy and also apparent from Fig. 11 it is observed that the oscillating crack growth pattern forms after a certain propagation length, which may explain that the measured initial fracture toughnesses $G_{Ic,o}$ across the different off-axis configurations, see Fig. 10, are similar. Similar observation was done by [32] in the study of pure cross-ply laminates where crack propagation in the 90° plies was oscillating between adjacent 0° plies.

From Fig. 11 it is also noted that the initiation of intraply delamination, i.e. migration from initial interlaminar delamination, depends of the off-axis angle $\theta$. Systematically across all off-axis DCB specimens tested, the migration correlates with the location of the off-axis fibers not supported and embedded in the initial crack of the DCB specimens, see Fig. 13. Since

| Specimen | Off-axis angle | $G_{Ic,o}$ [J/m$^2$] | $G_{Ic,max}$ [J/m$^2$] |
|---|---|---|---|
| 5.1 | 0° | 642 | 2295 |
| 5.2 | 0° | 469 | 2185 |
| 5.3 | 0° | 785 | 2302 |
| 5.4 | 0° | 594 | 2335 |
| 6.1 | 30° | 882 | 2702 |
| 6.2 | 30° | 581 | 2578 |
| 6.3 | 30° | 662 | 2682 |
| 6.4 | 30° | 1031 | 2547 |
| 7.1 | 60° | 966 | 2672 |
| 7.2 | 60° | 852 | 2618 |
| 7.3 | 60° | 770 | 2738 |
| 7.4 | 60° | 931 | 3063 |
| 7.5 | 60° | 802 | 2711 |
| 8.1 | 90° | 754 | 2579 |
| 8.2 | 90° | 784 | 2728 |
| 8.3 | 90° | 493 | 2725 |
| 8.4 | 90° | 812 | 2737 |
| 8.5 | 90° | 820 | 2543 |

Table 3: Calculated initial fracture toughness $G_{Ic,o}$ and the maximum fracture toughness $G_{Ic,max}$ for all layup design 2 specimens.

the transition from interlaminar to intraply delamination depends on the off-axis angle this also explains the sudden drop in fracture resistance and unstable crack growth for the 30° off-axis configuration, see Fig. 10, as the crack migration happens late. During the test the unstable crack growth of the 30° off-axis DCB specimens, due to sudden drop in fracture resistance, was observed to be associated with the transition. At crack migration a high amount of fiber bridging was suddenly lost. At further intraply delamination some fiber bridging was restored and fracture resistance increased as shown in Fig. 10. The fracture resistance curves of the 30° off-axis configurations did not reach a steady-state value since the test was stopped prematurely in order not to have crack propagation near the roller support structure of the test fixture invalidating the test results.

## 4. Conclusion

In the present paper, experimental testing of off-axis delamination of GFRP laminated DCB specimens have been conducted in order to better understand the delamination fracture process of more general and realistic laminate configurations as a step towards the development of general characterization and predictive methods for 3D delamination of real laminated composite structures. For that purpose two laminate layup designs have been considered in various configurations resulting in different off-axis angles having the interface crack growth direction off-axis to surrounding ply orientation. A special purpose delamination test fixture has been applied that enables DCB specimens to be loaded by pure uneven bending moments rendering the fracture resistance independent of the crack length. The off-axis delamination test of the various configurations resulted in complex fracture processes having very different fracture morphology.

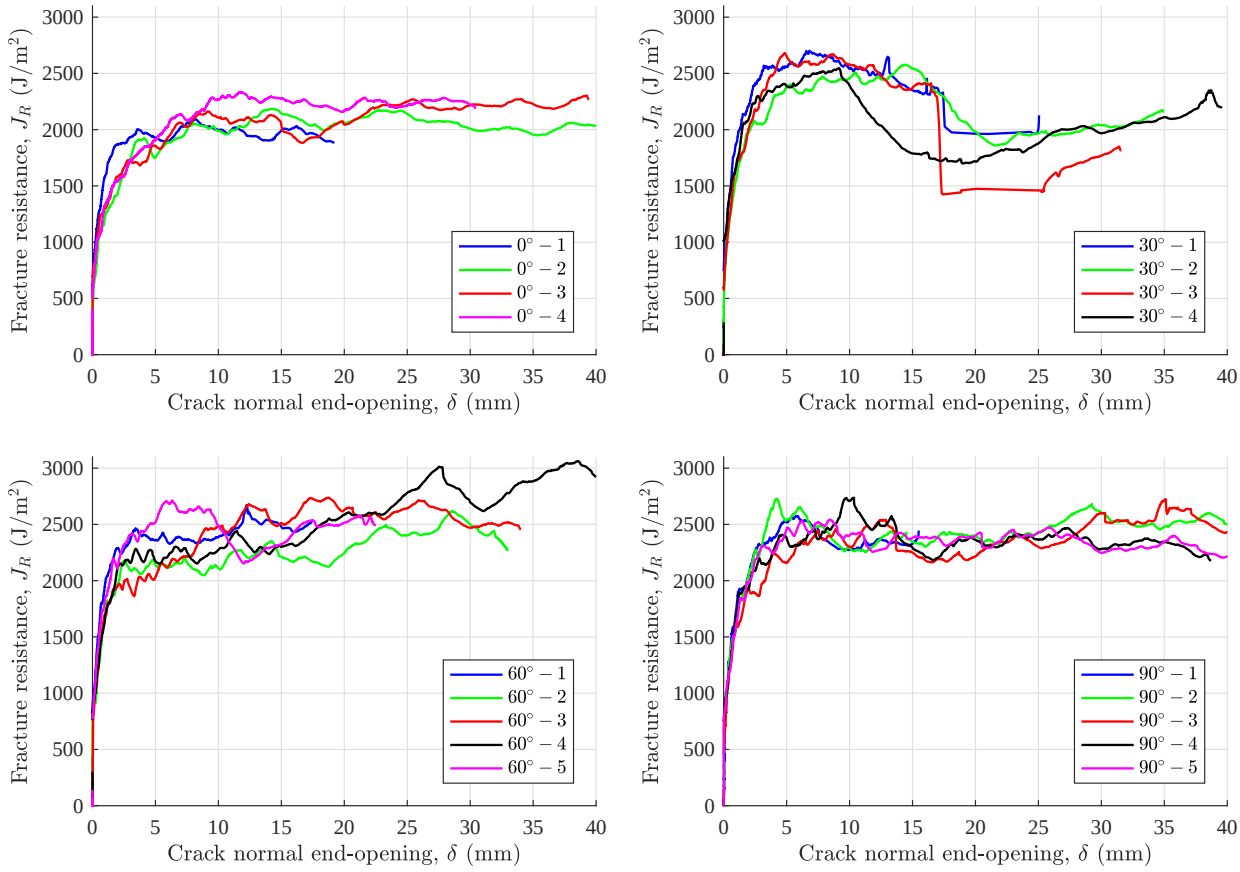


Figure 10: Fracture resistance curves for layup design 2 in four off-axis configurations $\theta = \{0°, 30°, 60°, 90°\}$.

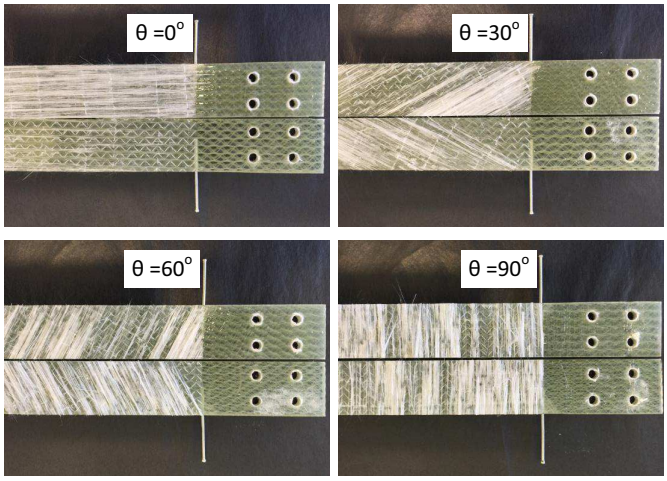


Figure 11: Typical fracture surfaces of layup design 2 with off-axis angles $\theta = \{0°, 30°, 60°, 90°\}$.

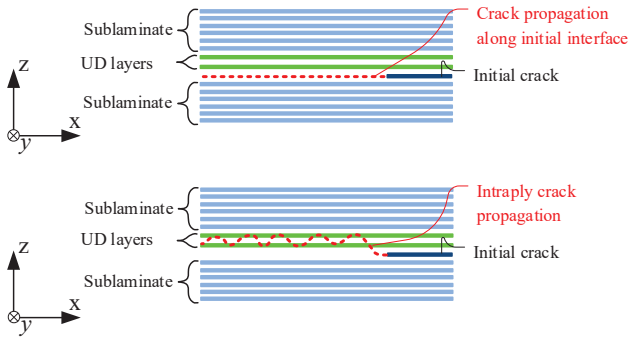


Figure 12: Illustration of the crack migration during crack propagation of DCB specimens of layup design 2. Top: Interlaminar delamination at specific UD@0°//BIAX@0° interface observed $\theta = 0°$ off-axis DCB specimens. Bottom: Intralaminar delamination with oscillating crack propagation in off-axis UD plies. Observed in all off-axis DCB specimens, i.e. $\theta = \{30°, 60°, 90°\}$.

In layup design 1 having the initial crack located at an interface surrounded by UD plies angled at two off-axis configurations $\theta = \{0°, 90°\}$ showed clear difference in initial fracture toughness $G_{Ic,o}$ under mode I loading. For the 90° off-axis configuration crack migration to an interface bounded by a 0° ply was observed.

In layup design 2 having the initial crack located at an interface surrounded by a 0° ply of a BIAX mat and UD plies angled at four off-axis configurations $\theta = \{0°, 30°, 60°, 90°\}$ and subjected to mode I loading showed complicated fracture phenomena. For all configurations, an insignificant difference in initial fracture toughness, $G_{Ic,o}$, and steady-state fracture toughness, $G_{Ic,ss}$, respectively, were measured. However, the fracture process among the different configurations was very different. The fracture process of all configurations started as interlaminar delaminations. For the non off-axis configuration, $\theta = 0°$,

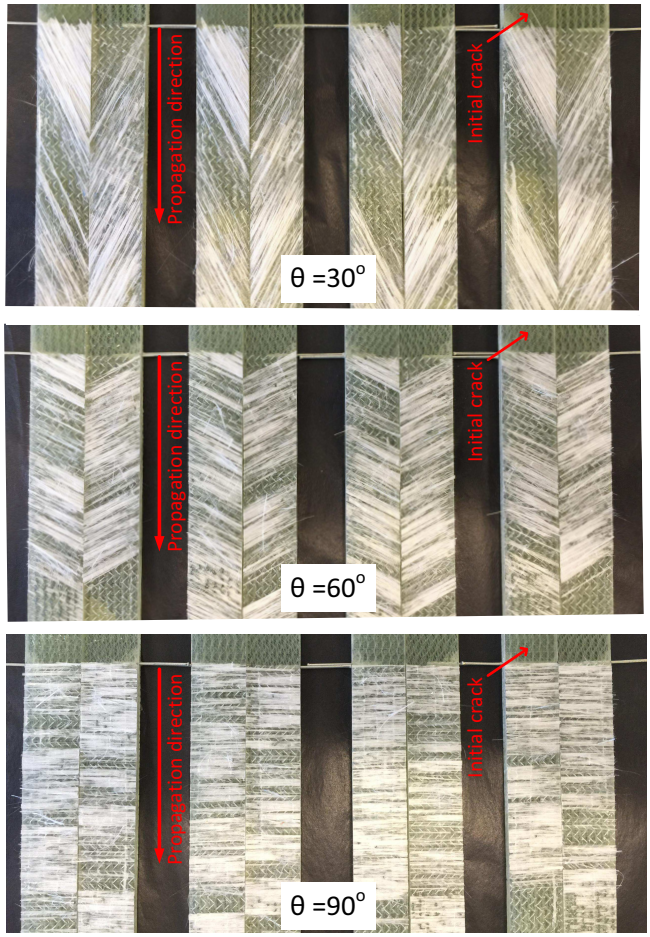


Figure 13: Fractography of off-axis DCB specimen configurations, i.e. $\theta = \{30°, 60°, 90°\}$. Crack traveling is systematically prohibited in all specimen until crack has propagated passed the UD fibers supported by the initial crack.

crack propagation continued as interlaminar. For all off-axis configurations $\theta = \{30°, 60°, 90°\}$, after a certain crack propagation length the delamination crack changed to intraply crack propagation as an oscillating crack within the off-axis UD plies, oscillating between the adjacent 0° plies of the BIAX mats. The transition from interlaminar to intraply crack propagation correlates with the location of off-axis fibers of the UD plies not embedded and supported by the initial crack of the DCB specimens. Thus, this indicates that the transition effects might be caused by free edge effects of the DCB specimens and not necessarily a real phenomenon in 3D delamination. At small off-axis angles the transition to intraply crack propagation happened late, i.e. after significant crack growth, and is associated with sudden drop in fracture resistance due to loss of fiber bridging. At further crack propagation some fiber bridging and thus fracture resistance is regained.

State-of-the-art cohesive zone models for prediction of delaminations in general 3D laminated composite structures implicitly assume isotropic fracture properties within the delamination plane as well as that the delaminations remain in the original crack plane. The current experimental study clearly demonstrates that that these assumptions are invalid in 3D delamination of a general interface of a laminate composite and thus should be carefully considered and understood in order to formulate more realistic predictive tools. For interfacial delamination between two UD plies very different initial fracture toughnesses were measured depending on the off-axis angle invalidating the assumption of isotropic fracture properties. For intraply crack propagation investigated in layup design 2 almost identical initial and steady-state fracture toughness, respectively, were measured over the studied off-axis configurations. Thus, for this particular laminate layup and material system the assumption about isotropy seems to be satisfied in cases of intraply crack propagation. However, the experimental results proved crack migration to be of high importance and that the typical assumption about delamination at a certain crack plane indeed is a rare case.

The detected crack migration during delamination testing of all off-axis configurations is speculated to be related to free edge effects of the 2D DCB specimens. Further research on characterization of crack migration is needed and it is suggested to be studied either by considered a sequence of DCB specimens of different width or by delamination test of a laminated composite plate with a circular delamination at an interface between unidirectional plies.

## Acknowledgements

The authors want to acknowledge Jon Svenninggaard who as a part of his M.Sc. thesis project dimensioned the presented pure uneven moment loaded test fixture for mixed mode fracture characterization of double cantilever beam specimens.

[1] N. J. Pagano, G. A. Schoeppner, Delamination of polymer matrix composites: problems and assessment, Comprehensive composite materials 2 (2000) 433–528.
[2] ASTM D5528-13(2013), Standard Test Method for Mode I lnterlaminar Fracture Toughness of Unidirectional Fiber-Reinforced Polymer Matrix Composites, Tech. rep., ASTM International, www.astm.org (2013).
[3] G. Beer, An isoparametric joint/interface element for finite element analysis, International Journal for Numerical Methods in Engineering 21 (4) (1985) 585–600.
[4] A. Gens, I. Carol, E. Alonso, An interface element formulation for the analysis of soil-reinforcement interaction, Computers and Geotechnics 7 (1-2) (1989) 133–151.
[5] H. Schellekens, R. Borst, Geometrically and physically non-linear interface elements in finite element analysis of layered composite structures, in: J. Füller, G. Grüninger, K. Schulte, A. R. Bunsell, A. Massiah (Eds.), Developments in the Science and Technology of Composite Materials, Springer Netherlands, 1990, pp. 749–754.
[6] M. Ortiz, A. Pandolfi, Finite-deformation irreversible cohesive elements for three-dimensional crack-propagation analysis, International Journal for Numerical Methods in Engineering 44 (9) (1999) 1267–1282.
[7] A. de Andrés, J. L. Pérez, M. Ortiz, Elastoplastic finite element analysis of three-dimensional fatigue crack growth in aluminum shafts subjected to axial loading, International Journal of Solids and Structures 36 (15) (1999) 2231–2258.
[8] S. R. Chowdhury, R. Narasimhan, A cohesive finite element formulation for modelling fracture and delamination in solids, Sadhana Academy Proceedings in Engineering Sciences 25 (2000) 561–587.
[9] G. Alfano, M. A. Crisfield, Finite element interface models for the delamination analysis of laminated composites: mechanical and computational issues, International Journal for Numerical Methods in Engineering 50 (7) (2001) 1701–1736.
[10] P. P. Camanho, C. G. Davila, M. F. de Moura, Numerical simulation of mixed-mode progressive delamination in composite materials, Journal of Composite Materials 37 (16) (2003) 1415–1438.

[11] A. Turon, P. P. Camanho, J. Costa, C. G. Dávila, A damage model for the simulation of delamination in advanced composites under variable-mode loading, Mechanics of Materials 38 (11) (2006) 1072–1089.
[12] B. L. V. Bak, E. Lindgaard, E. Lund, Analysis of the integration of cohesive elements in regard to utilization of coarse mesh in laminated composite materials, International Journal for Numerical Methods in Engineering 99 (8) (2014) 566–586.
[13] E. Lindgaard, B. Bak, J. Glud, J. Sjølund, E. Christensen, A user programmed cohesive zone finite element for ansys mechanical, Engineering Fracture Mechanics 180 (2017) 229 – 239. doi:https://doi.org/10.1016/j.engfracmech.2017.05.026.
[14] L. Carreras, B. Bak, A. Turon, J. Renart, E. Lindgaard, Point-wise evaluation of the growth driving direction for arbitrarily shaped delamination fronts using cohesive elements, European Journal of Mechanics - A/Solidsdoi:https://doi.org/10.1016/j.euromechsol.2018.05.006.
[15] J. Andersons, M. König, Dependence of fracture toughness of composite laminates on interface ply orientations and delamination growth direction, Composites Science and Technology 64 (13-14) (2004) 2139 – 2152. doi:http://dx.doi.org/10.1016/j.compscitech.2004.03.007.
[16] A. Russell, K. Street, Factors affecting the interlaminar fracture energy of graphite/epoxy laminates, in: Proceedings of ICCM IV, 1982, pp. 279–300.
[17] R. Olsson, J. Thesken, F. Brandt, N. Jönsson, S. Nilsson, Investigations of delamination criticality and the transferability of growth criteria, Composite Structures 36 (3-4) (1996) 221 – 247. doi:http://dx.doi.org/10.1016/S0263-8223(96)00079-7.
[18] K. Trakas, M. Kortschot, The relationship between critical strain energy release rate and fracture mode in multidirectional carbon-fiber/epoxy laminates, in: Composite Materials: Fatigue and Fracture, Vol. 6, ASTM STP 1285, 1997, pp. 283–304, ISBN 0-8031-2411-2.
[19] L. Yong, L. Shunling, X. Jun, T. Jie, Study on the mode I interlaminar fracture toughness of multi-directional laminates, in: Proceedings of ICCM 11, Vol. 2, 1997, pp. 431–437.
[20] O. Allix, D. Lévêque, L. Perret, Identification and forecast of delamination in composite laminates by an interlaminar interface model, Composites Science and Technology 58 (5) (1998) 671 – 678. doi:http://dx.doi.org/10.1016/S0266-3538(97)00144-9.
[21] F. Lachaud, R. Piquet, L. M. L, Delamination in mode I and II of carbon fibre composite materials: fibre orientation influence, in: Proceedings of ICCM-12, 1999.
[22] W. Jordan, Changing the toughness of graphite fiber/resin based composites by changing their internal structure, Composites Part B: Engineering 31 (3) (2000) 245 – 252. doi:http://dx.doi.org/10.1016/S1359-8368(00)00008-1.
[23] A. Laksimi, M. Benzeggagh, G. Jing, M. Hecini, J. Roelandt, Mode i interlaminar fracture of symmetrical cross-ply composites, Composites Science and Technology 41 (2) (1991) 147 – 164. doi:http://dx.doi.org/10.1016/0266-3538(91)90025-K.
[24] B. W. Kim, A. H. Mayer, Influence of fiber direction and mixed-mode ratio on delamination fracture toughness of carbon/epoxy laminates, Composites Science and Technology 63 (5) (2003) 695 – 713. doi:http://dx.doi.org/10.1016/S0266-3538(02)00258-0.
[25] T. Sebaey, N. Blanco, J. Costa, C. Lopes, Characterization of crack propagation in mode i delamination of multidirectional {CFRP} laminates, Composites Science and Technology 72 (11) (2012) 1251 – 1256. doi:http://dx.doi.org/10.1016/j.compscitech.2012.04.011.
[26] B. F. Sørensen, T. K. Jacobsen, Characterizing delamination of fibre composites by mixed mode cohesive laws, Composites Science and Technology 69 (3-4) (2009) 445–456.
[27] J. Svenninggaard, B. Bak, J. Andreasen, E. Lindgaard, Test fixture for double cantilever beam specimens subjected to uneven bending moments, Submitted for review.
[28] B. Sørensen, K. Jørgensen, T. Jacobsen, R. Østergaard, DCB-specimen loaded with uneven bending moments, International Journal of Fracture 141 (1) (2006) 163–176.
[29] J. W. Hutchinson, Z. Suo, Mixed Mode Cracking in Layered Materials, ADVANCES IN APPLIED MECHANICS 29.
[30] B. F. Sørensen, P. Kirkegaard, Determination of mixed mode cohesive laws, Engineering Fracture Mechanics 73 (17) (2006) 2642 – 2661. doi:https://doi.org/10.1016/j.engfracmech.2006.04.006.
[31] PRO-SET Inc., `https://www.prosetepoxy.com/standard-products/infusion-epoxies/`, note = Accessed: 2018-05-23.
[32] A. Brunner, B. Blackman, P. Davies, A status report on delamination resistance testing of polymer-matrix composites, Engineering Fracture Mechanics 75 (9) (2008) 2779–2794. doi:10.1016/j.engfracmech.2007.03.012.